On the Availability of the Decoy State BB84 QKD over a Terrestrial FSO Link

Argiris Ntanos
School of Electrical and Computer Engineering
National Technical University of Athens
Athens, Greece
ntanos_arg@outlook.com

Dimitris Zavitsanos
School of Electrical and Computer Engineering
National Technical University of Athens
Athens, Greece
dimizavitsanos@mail.ntua.gr

Nikolaos K. Lyras
School of Electrical and Computer Engineering
National Technical University of Athens
Athens, Greece
lyrasnikos@mail.ntua.gr

Giannis Giannoulis
School of Electrical and Computer Engineering
National Technical University of Athens
Athens, Greece
jgiannou@mail.ntua.gr

Hercules Avramopoulos
School of Electrical and Computer Engineering
National Technical University of Athens
Athens, Greece
hav@mail.ntua.gr

***Abstract*—A research contribution focusing on the feasibility of the Decoy State BB84 Quantum Key Distribution (QKD) protocol over a free-space optical (FSO) link under strong and moderate solar radiance in the urban environment of Athens city, Greece for short distances up to 1km is presented. Emphasis is placed on the time varying attenuation which is introduced by various atmospheric processes and especially on the effect of strong atmospheric turbulence. We examine how these factors affect the performance of the FSO link by conducting numerical simulations of the Secure Key Rate (SKR) and evaluating the link availability.**

***Index Terms*—QKD, Terrestrial FSO, Turbulence**

I. Introduction

With the recent advancements in Quantum Computing Technologies, the necessity of a high-security level for storing and transmitting sensitive information has become even more topical. The advent of powerful quantum computers could set a large part of our cryptosystems totally insecure leading to very serious consequences. Fortunately, quantum mechanics has provided the tools to combat this threat. Quantum Key Distribution (QKD) offers a key exchange whose security is based on the laws of nature and promises in principle unconditional security [1].

Since the first demonstration of a QKD protocol in 1984 by Bennett and Brassard, known as the BB84 protocol [2], QKD has rapidly developed over the last years and the distance between the two trusted nodes (Alice, Bob) has been increased significantly, using not only fiber as a medium but also free space as a wireless link [3], achieving high Secure Key Rates (SKR) even at large distances. Specifically, over the last years, notable steps have been made towards a highly secure global communication network, by exploiting QKD in satellites communications using Free Space Optical (FSO) links [4]. Besides these long-range quantum links, successful QKD over terrestrial FSO links have been deployed, demonstrating the experimental evidence of Point-to-Point (P2P) quantum links in sub-km scale [5], [6]. These links can be realized exploiting the legacy infrastructure of classical FSO links combined with the compatible single-photon sources and detectors. From a deployment perspective, the emergence of FSO links in support of mobile transport pipes for 5G and beyond systems [7] allow for an inherently compatible infrastructure for implementing QKD links. Moreover, unlike the challenges that the fiber medium imposes to the transmission of weak, quantum signals (e.g., high loss, dispersion effects, noise from intense data streams in shared fiber configurations), FSO links can be considered as an attractive physical layer for the quantum distribution. On the other hand, FSO links have to overcome the environmental degradation, not only from the high background solar noise but also by the time varying attenuation caused by the weather conditions and especially the scintillation effect.

While the majority of the already published research [8] is mainly focused on the challenge of increasing the FSO link distance, the feasibility of short terrestrial real-world QKD over FSO implementations under various atmospheric effects has not been extensively examined. Based on a very interesting study emphasizing on the scintillation effect in the time-varying FSO channel on QKD systems [9], we take a step forward by presenting an extended study including additional time varying atmospheric processes. In more detail, we model and optimize the FSO link for a reference distance of 300m taking into account the time varying attenuation that is introduced by reduced visibility, rain and strong turbulence as well as the solar induced background noise. By obtaining realistic atmospheric data from the location of Athens, Greece we translate the variations of these four processes into QKD link availability. Finally, we present performance evaluation results for longer distances, reporting a normalized value of Secure Key Rate (SKR/f_{rep} $(bits/pulse)$), where f_{rep} is Alice's repetition rate, higher than $2\text{x}10^{-6}$ with 99% availability for

978-3-903176-33-1

a link distance of $1km$.

This paper is organized as follows. In sections II and III, we briefly present the basic methodology for QKD and the modeling of the FSO link. Section IV provides the selection and optimization of the setup components as well the results of our study. Finally, section V concludes this work.

II. Weak + Vacuum BB84 Decoy State Protocol

A typical inter-building P2P FSO link, over which we evaluated the performance of a Discrete Variable (DV)-QKD, is shown in Fig. 1. In our simulations, we considered the most well-known QKD protocol, the BB84 protocol [2]. Even though its unconditional security has been proved by exploiting the laws of quantum mechanics [10], [11], the security loopholes that arise from the real-world, non-idealized implementation of these protocols has led the scientific community to invent and implement more resilient schemes [12]. One of the most common security concerns arises from the substitution of single-photon sources by attenuated coherent laser sources. The Poissonian distribution that the coherent states obey implies that some of the output pulses may contain multiple photons, even if the mean photon number is kept below 1. The vulnerability of these pulses to photon number splitting (PNS) attacks can cause a significant security problem, limiting thereby the secure key distribution distance [13]. The most famous modification of the BB84 protocol in order to enhance the robustness against this kind of attacks is to introduce decoy states. It has been shown that with the so-called decoy state QKD BB84 protocol, long communication distances and high key rates can be achieved [14], increasing thereby the robustness of QKD technology. Nowadays, the decoy state BB84 is widely implemented in many QKD demonstrations, validating its practicality and it's superior performance [15].

For these reasons, we adopted the phase coding weak+vacuum decoy BB84 protocol [16]. In this version of the decoy state QKD, Alice prepares and transmits randomly to Bob three different states: one signal state and two decoy states (one of which is the vacuum state). The introduction of the two decoy states enables the detection of eavesdropping via the PNS attack and leads to comparatively higher normalized SKR [14]:

$$SKR/f_{rep} \geq q\{Q_1[1 - H_2(e_1)] - Q_\mu f(E_\mu)H_2(E_\mu)\}, \quad (1)$$

where q is the protocol efficiency, the subscript μ is the average photon number per signal in signal states, Q_μ and E_μ are the gain and the quantum bit error rate (QBER) of signal states, respectively, Q_1 and e_1 are the gain and the error rate of the single photon state in signal states, respectively, $f(x)$ is the bi-directional error correction rate and $H_2(x)$ is the binary entropy function. In a real experiment, Q_μ and E_μ are measurable quantities, while Q_1 and e_1 should be estimated. With the weak+vacuum decoy BB84 protocol one can obtain tight bounds for Q_1 and e_1, which can be used to lower-bound the SKR [14].

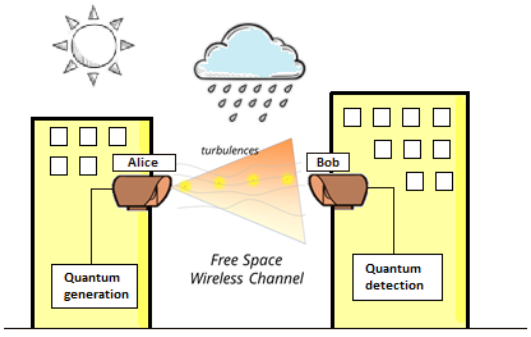

Fig. 1. QKD over FSO inter-building link.

III. Free Space Channel

The performance of the free space optical communication systems is severely affected by the atmospheric conditions. In the following sub-sections, the constant and time varying atmospheric losses are summarized.

A. Time Independent Channel Losses

1) Geometrical Loss: As the laser beam propagates through the atmosphere its diameter expands resulting in a spot diameter d_s (m) at the receiver given by [7]: $d_s = d_t + 2L\tan(\Theta/2)$, where d_t (m) is the transmitter lens diameter, Θ $(mrad)$ corresponds to the divergence of the beam and L (km) is the link distance. The geometrical losses due to the enlarged beam are given in dB by [7]:

$$A_{geo} = 10\log_{10}(a_r/d_s)^2, \quad (2)$$

where a_r (m) is the receiver's aperture diameter. According to [17], when the link is short enough, the capture area can be greater than the beam area ($a_r > d_s$), resulting that all of the beam is collected. In these cases, the geometrical loss can be set to zero.

2) Clear Air Loss: Under clear air conditions (absence of fog, rain, turbulence etc.) the attenuation occurs mainly due to absorption by gaseous molecules. Specific clear air attenuation for this wavelength is generally low and can be given in dB by [9]:

$$A_{clear} = 10\log_{10}(e^{-\beta L}), \quad (3)$$

in which $\beta = a/4.3429$ based on Beer-Lambert law and $a = 0.192$ [9] is the attenuation coefficient measured in dB/km for the wavelength of $1550nm$.

B. Time Dependent Channel Losses

1) Atmospheric Turbulence: Turbulence can heavily affect FSO communication systems causing intensity fluctuations in the receiver known as scintillation. These fluctuations occur due to changes in the refractive indices in small air cells that are caused by thermal changes. Parts of the laser beam are diffracted towards different directions resulting in a decreased power level at the receiver [3].

The intensity of the scintillation is often described as weak, moderate and strong depending on the value of the refractive index structure parameter ${C_n}^2$ $(m^{-2/3})$ that may vary from values between 10^{-17} and 10^{-12} [17]. In the case of weak and moderate turbulence (${C_n}^2 < 10^{-13}$), scintillation effects can be modeled according to the log-normal distribution as described in [18]. In the case of strong turbulence (${C_n}^2 \geq 10^{-13}$), the Gamma-Gamma distribution is more suitable. In this analysis we are focused on strong turbulence. Using the Gamma-Gamma distribution, the normalized intensity (I) can be divided to the effect of large scale and small scale eddies (I_x, I_y), with each one following a Gamma distribution considering that the total intensity I equals to $I = I_x I_y$ [3]. The normalized probability density function (PDF) of the light intensity (I) reaching the receiver is given by [9]:

$$f(I) = \frac{2(ab)^{(a+b)/2}}{\Gamma(a)\Gamma(b)}\ I^{\frac{(a+b)}{2}-1}\ K_{a-b}(2\sqrt{abI}), \qquad (4)$$

where a and b are the effective number of large scale and small scale turbulent eddies, $\Gamma(\cdot)$ is the gamma function and K_{a-b} is the modified Bessel function of second kind of order $(a-b)$. The distribution shaping parameters a, b can be expressed as [19]:

$$a = (\exp[\frac{0.49\ \sigma_r^2}{(1+0.18d^2+0.56\sigma_r^{12/5})^{7/6}}] - 1)^{-1} \qquad (5)$$

$$b = (\exp[\frac{0.51\sigma_r^2(1+0.69\sigma_r^{12/5})^{-5/6}}{(1+0.9d^2+0.62\sigma_r^{12/5})^{5/6}}] - 1)^{-1}, \qquad (6)$$

where ${\sigma_r}^2 = 1.23\ {C_n}^2 k^{7/6} L^{11/6}$ is the Rytov variance [3] and $d = \sqrt{(k\ {a_r}^2)/(4L)}$ where $k = (2\pi)/\lambda$ is the optical wave number. Therefore, the attenuation (dB) introduced due to the effect of scintillation for a given threshold probability p_{th} (e.g 0.1, 0.01 etc.), $A_{sci}(p_{th})$, can be derived from the cumulative distribution function (CDF) as follows:

$$CDF(I) = G(I) = \int_{-\infty}^{p_{th}} f(I)\, dI \qquad (7)$$

$$A_{sci}(p_{th}) = 10\log_{10}[G^{-1}(I)]. \qquad (8)$$

2) Scattering: Light that travels through the atmosphere is scattered by the particles and molecules resulting in a loss of signal. The main scattering process is Mie scattering, which occurs due to the presence of fog, haze and aerosol particles, since the size of these molecules is at the same scale with the laser wavelength. Mie scattering coefficient is usually approached as related to the visibility [17]. A widely used empirical formula to calculate the specific attenuation caused by Mie scattering in (dB/km) is [17]:

$$\gamma_{scat}(\lambda) = \frac{3.91}{V}\left(\frac{\lambda}{550nm}\right)^{-q}, \qquad (9)$$

where V (km) is the visibility, λ (nm) is the optical wavelength and q is a coefficient dependent on the size distribution of the scattering particles that is given by the Kim model [7].

3) Rain attenuation: For calculating the attenuation due to rainfall we assume that the raindrops have a spherical shape. In this case, specific rain attenuation (dB/km) is given by the equation [17]:

$$\gamma_{rain} = kR^a, \qquad (10)$$

where R (mm/hr) is the rain rate and the values of the parameters k, a for the wavelength of $1550nm$ were obtained by [20] assuming a shape parameter of 1.

4) Solar background noise: One of the biggest challenges in the implementation of a QKD FSO link under daylight conditions is the solar induced background noise in the receiver, since single photon detectors are extremely sensitive to noise. The background noise power level in Watt reaching the receiver can be given by [21]:

$$P_{back} = H_{rad}\Omega_{FOV}A_r\Delta\lambda, \qquad (11)$$

where H_{rad} $(W/m^2 sr\mu m)$ corresponds to the background radiance energy density coming directly or indirectly from the sun or other sources, Ω_{FOV} (sr) is the field of view of the receiver's aperture, A_r (m^2) is the receiver's capture area and $\Delta\lambda$ (μm) is the receiver's band pass optical filter width. It is evident by eq. (11) that in order to decrease the solar radiance we can select a narrow field of view (FOV) and also compromise the receiver's aperture to properly balance the background noise and scintillation effect. It is also important to consider that in the case of a terrestrial FSO system the link is usually horizontal, therefore the receiver is not directed towards the sky. In order to reduce the solar interference, it is also possible to arrange the link direction so that the sun is always off axis.

IV. Results

A. FSO System Parameters

The link parameters are selected in order for the performance of the QKD over FSO to be optimized in terms of SKR at a reference distance of $300m$. The selected parameters are kept the same for the whole simulation analysis and numerical results. To begin with, in our study the selected wavelength is $1550nm$ which guarantees high atmospheric transmittance and decreased solar radiance [21], [22]. Concerning the setup components, we considered a transmitter's aperture of $50mm$ [23], a narrow beam divergence of $0.182mrad$ [24] and a receiver's aperture of $180mm$ [25]. With the selected beam parameters, the geometrical loss is zero for distances shorter than $700m$. The receiver's aperture diameter was optimally selected, balancing the contribution of turbulence and background solar counts at the reference distance. To continue, for the minimization of the effects of solar irradiance, a narrow band-pass filter with a bandwidth of $1nm$ and a FOV of $283\mu rad$ as in [6] were assumed. The receiver's FOV is big enough to capture the whole beam divergence but also limited as possible to constrain the background irradiance. The rest of the values that are related to the loss of the FSO system components and the decoy state QKD are listed in table I.

TABLE I
SYSTEM PARAMETERS

System parameter	Value
Detection efficiency[a]	10%
Detector's dead time t_{dead}[a]	$20\mu s$
Detector's gate duration time Δ_t[a]	$1ns$
Bob's interferometer visibility[a]	98%
Detector's dark count rate (DCR)[a]	$10^3 cps$
After-pulse probability factor ρ_{ap}[a]	0.008
Bob's receiver's loss[a]	$2.65dB$
Bi-direction error correction efficiency $f(e)$ [b]	1.2
$1nm$ band pass filter loss[c]	$3dB$
Housing loss[d]	$1.5dB$
Misalignment loss	$0.5dB$

Values obtained from [a] [26] ,[b] [14], [c] [6],[d] [7] .

Finally, the quantum signal mean value $\mu = 0.439$, the decoy signal mean value $\nu = 0.11$ and the protocol efficiency $q = 1/3$ [14] were also optimized in order to maximize the SKR at the distance of $300m$.

B. FSO Channel Assumptions

In this sub-section, the assumptions and considerations for the FSO channel are summarized. Firstly, in our analysis strong turbulence is assumed with the value of ${C_n}^2$ set to 10^{-12} $(m^{-2/3})$. The effect of turbulence on the FSO link for different probability thresholds is estimated employing Gamma-Gamma distribution as described in section III. Regarding the effect of rainfall, rain rate values for different percentage levels for Athens are obtained from the complementary cumulative distribution function (CCDF) presented in [27], where real rain rate data for two years period are presented. The rain attenuation is estimated for different thresholds according to section III. To continue, the visibility is set to the constant value of $6km$ that corresponds to a value below than the average daily visibility of Athens $(9km)$ [28], which ensures that visibility introduced attenuation is always taken into account. Finally, for the estimation of the background noise during the daytime the value of solar radiance is assumed as 0.2 $W/m^2 sr\mu m$ as derived from [29]. This value is also considered as the maximum daylight radiance in [5]. For our link assumptions, this value corresponds to a background noise of $50K$ counts per second (cps).

C. Numerical Analysis over Daylight Conditions

The QKD over FSO link is evaluated for the distances of $300m$, $600m$, $800m$ and $1000m$ in terms of link attenuation threshold (dB) and availability in daylight (full radiance). Assuming that all components losses are constant and considering that geometrical and clear atmospheric losses do not vary in time, the attenuation threshold denotes the maximum additional loss that may be introduced by time varying atmospheric processes such as reduced visibility, rain and turbulence without completely interrupting the link. Assuming that all three atmospheric processes are independent (worst case scenario), we calculate the maximum value of attenuation in dB that can be introduced to the FSO link for outage thresholds ranging from 90% to 99.999%.

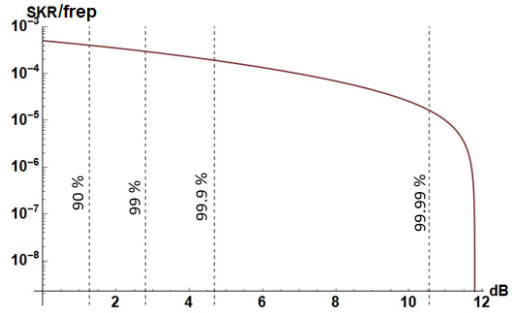

Fig. 2. Normalized SKR over additional atmospheric attenuation (dB) for a link distance of $300m$ under daylight conditions. The vertical lines refer to the maximum value of attenuation that is introduced by reduced visibility, rain and strong turbulence for outage thresholds 90%, 99%, 99.9%, 99.99%.

Fig. 2 shows the normalized SKR over the additional attenuation that can be introduced by reduced visibility, rain and strong turbulence in dB for a link distance of $300m$. At zero dB the maximum normalized value of the SKR that includes all setup components losses, as well as geometrical and clear air attenuation loss is obtained, while the value of about $11.8dB$ corresponds to the attenuation threshold for this distance. The link can remain uninterrupted at least for the 99.99% of the time under full daylight conditions under the

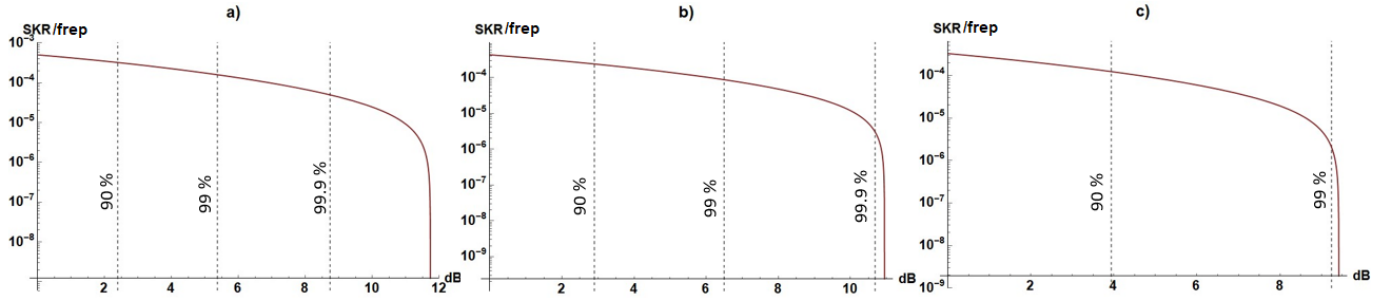

Fig. 3. Normalized SKR over additional atmospheric attenuation (dB) for link distances of a) $600m$, b) $800m$, c) $1000m$, under daylight conditions. The vertical lines refer to the maximum value of attenuation that is introduced by reduced visibility, rain and strong turbulence for outage thresholds 90%, 99%, 99.9%.

influence of strong turbulence with an additional link margin of about $1.2dB$.

Fig. 3 shows the normalized SKR over the attenuation that can be introduced by reduced visibility, rain and strong turbulence in dB for link distances of 600, 800 and $1000m$. The difference between the attenuation threshold in fig. 2 and fig. 3a) is insignificant (about $11.8dB$ in both) due to the weak influence of clear air attenuation. On the other hand, in fig. 3 b), 3 c) it may be observed that this threshold is significantly reduced, since the influence of geometrical loss affects now the link severely. At $800m$ it can be observed a decreased attenuation threshold of about $10.9dB$. Even further, at the distance of $1km$ it is observed that the attenuation threshold is reduced to only $9.4dB$, thus hardly achieving an availability of 99% with very low SKR and no additional link margin.

D. Numerical Analysis over Reduced Radiance

In this part, the performance of the link under reduced background noise or nighttime conditions is studied. It is mentioned that absolute zero background noise is not achievable even during the night, since city lights or night sky will introduce a small amount of noise.

The contour plot of the SKR for background noise up to $50Kcps$ (maximum radiance) for the distance of $300m$ is given in fig. 4. At lower background noise the link tolerance in attenuation introduced by visibility, rain and turbulence increases, resulting in a greater attenuation threshold, thus reaching higher values of availability. The maximum achievable attenuation threshold assuming that background noise is set to zero, is calculated to be about $25dB$. Fig. 4 shows that availability up to 99.999% under strong turbulence for background solar counts lower than $17Kcps$ can be achieved.

Fig. 5 shows the contour plot of the SKR for background noise up to $50Kcps$ for the distances of 600, 800 and $1000m$. As before, the influence of the geometrical loss appears only in fig. 5 b) and fig. 5 c) shifting the contours to the left, thus limiting the attenuation threshold. Under reduced background noise, it is possible to extend the availability from 99.9% to 99.99% for the distance of $600m$ and from 99% to 99.9% for the distances of $800m$ and $1000m$.

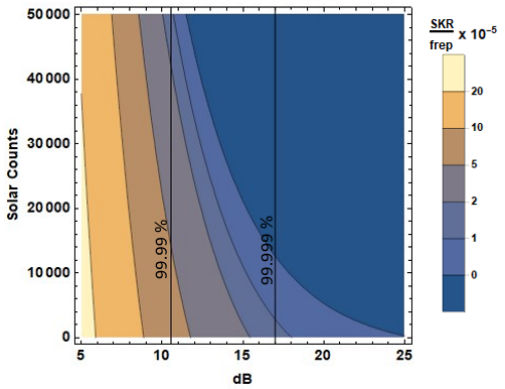

Fig. 4. Contour plot of the normalized SKR over additional atmospheric attenuation (dB) and background solar noise counts (cps) for a link distance of $300m$. The vertical lines refer to the maximum value of attenuation that is introduced by reduced visibility, rain and strong turbulence for outage thresholds 99.99%, 99.999%.

E. Numerical Analysis over Distance

Finally, the limit performance of the link in greater distances under daylight conditions is evaluated. Fig. 6 shows the contour plot of the normalized SKR over distance and over attenuation introduced by visibility, rain and turbulence. The contour line of $SKR = 0$ shows the dependence of the attenuation threshold over distance. It is shown that the maximum reach of the link is just above the distance of $3km$ with no additional link margin for this distance. The point in which the link attenuation threshold begins to fall quadratically (about $700m$) indicates the distance where geometrical loss begins to affect the link, thus making the setup much more vulnerable to atmospheric losses. For distances greater than $1km$ the attenuation threshold is already severely limited resulting in a less reliable link.

Given the meteorological data of each location, it is possible to statistically define the variation of the attenuation introduced

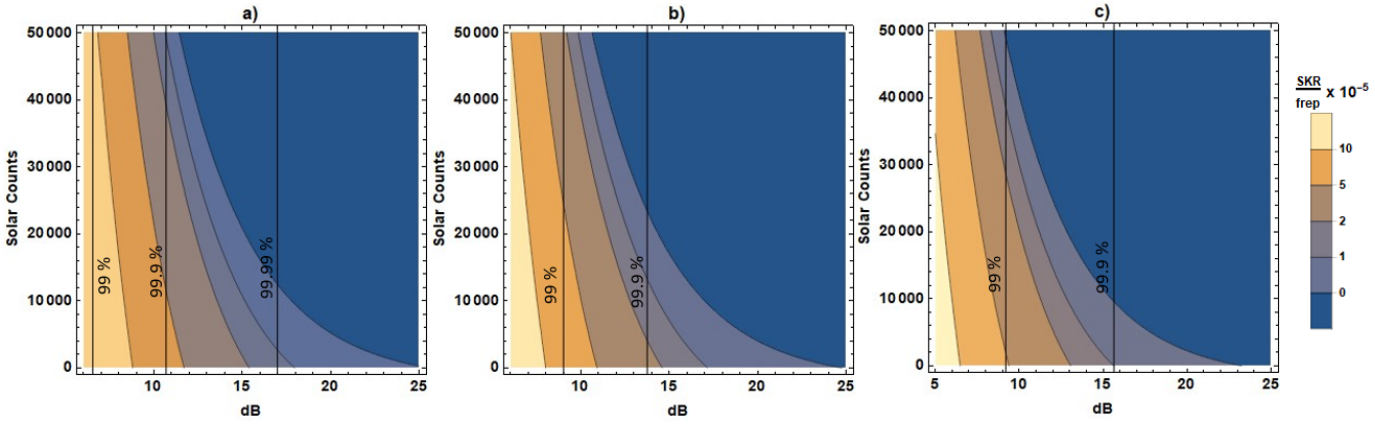

Fig. 5. Contour plot of the normalized SKR over additional atmospheric attenuation and background solar noise counts (cps) for link distances a) $600m$, b) $800m$, c) $1000m$. The vertical lines refer to the maximum value of attenuation that is introduced by reduced visibility, rain and strong turbulence for outage thresholds 99%,99.9%,99.99%.

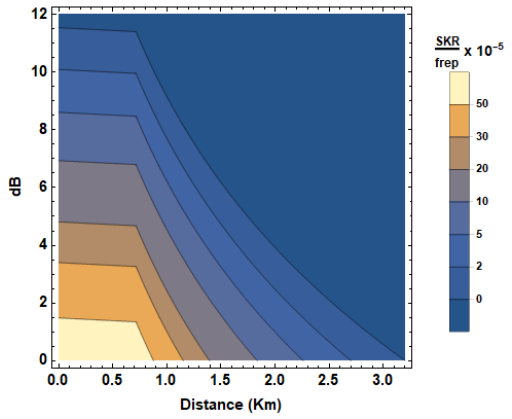

Fig. 6. Contour plot of the normalized SKR over additional attenuation (dB) introduced by reduced visibility, rain, turbulence and link distance (km) under daylight conditions.

by visibility, rain and turbulence, thus allowing us to estimate the maximum availability reach of a terrestrial QKD deployment for a given distance.

V. Conclusion

In this contribution, the feasibility of a sub-km terrestrial QKD over FSO implementation has been thoroughly examined. By taking into account the most important atmospheric processes that affect the QKD performance, we conducted numerical calculations of the SKR for the specific distance of $300m$, given the meteorological data of Athens city. Under these weather conditions, the reported results imply that the link can remain uninterrupted for long time periods under strong solar radiance, even under the presence of strong turbulence. Finally, we evaluated the performance of the same configuration for distances up to $1km$, concluding that such an implementation is feasible with reduced reliability. Combined with attenuated coherent sources emitting optical pulses at MHz-repetition rates, the distilled key rates of the reported FSO links meet the security specifications in various Point-to-Point (P2P) and Point-to-MultiPoint (P2MP) connectivity scenarios in the context of 5G and Beyond infrastructure [30]. The path towards hybrid fiber/FSO infrastructure for quantum symmetric key delivery can be also a deployment option for network segments where the optical fibers have not been installed, and thus sub-Km wireless optical links undertake to connect securely multiple mobile terminal nodes [31].

Acknowledgment

Part of the research leading to this work was also supported by the H2020-funded Flagship project UNIQORN (820474).

References

[1] Pirandola, S., Andersen, U. L., Banchi, L., Berta, M., Bunandar, D., Colbeck, R., & Wallden, P. (2020). Advances in quantum cryptography. Advances in Optics and Photonics, 12(4), 1012-1236.

[2] Bennett, C. H., and Gilles B. "Proceedings of the ieee international conference on computers, systems and signal processing." (1984).

[3] Andrews, L. C., and Ronald L. Phillips. "Laser beam propagation through random media." SPIE, 2005.

[4] Bedington, R., Arrazola, J. M., & Ling, A. Progress in satellite quantum key distribution. npj Quantum Information, (2017), 3(1), 1-13.

[5] Carrasco-Casado, A. , Fernández V., and Denisenko N. "Free-space quantum key distribution." Optical Wireless Communications. Springer, Cham, 2016. 589-607.

[6] Ko, Heasin, et al. "Daylight operation of a high-speed free-space quantum key distribution using silica-based integration chip and micro-optics-based module.", in Proc. of OFC 2019.

[7] Schulz, D. , et al. "Robust optical wireless link for the backhaul and fronthaul of small radio cells." Journal of Lightwave technology 34.6 (2016): 1523-1532.

[8] Trinh, P. V., et al. "Quantum key distribution over FSO: Current development and future perspectives." 2018 Progress in Electromagnetics Research Symposium (PIERS-Toyama). IEEE, 2018.

[9] Sun, X. , Ivan B. Djordjevic, and Mark A. Neifeld. "Secret key rates and optimization of BB84 and decoy state protocols over time-varying free-space optical channels." IEEE Photonics Journal 8.3 (2016): 1-13.

[10] Lo, H. K. & Chau, H. F. Unconditional security of quantum key distribution over arbitrarily long distances. Science 283, 5410 (1999).

[11] Shor, P. & Preskill, J. Simple proof of security of the BB84 quantum key distribution protocol. Phys. Rev. Lett. 85, 441–444 (2000).

[12] Diamanti, E.; Lo, H. K.; Qi, B.; Yuan, Z. Practical challenges in quantum key distribution. npj Quantum Information, 2016, 2(1).

[13] Mailloux, L.; Hodson, D.; Grimaila, M.; Engle, R.; McLaughlin, C.; Baumgartner, G. Using modeling and simulation to study photon number splitting attacks. IEEE Access 2016, 4, 2188–2197.

[14] Ma, X. , et al. "Practical decoy state for quantum key distribution." Physical Review A 72.1 (2005): 012326.

[15] Wang S., et al. "Field and long-term demonstration of a wide area quantum key distribution network." Optics express 22.18 (2014): 21739-21756.

[16] Zhao, Yi, et al. "Simulation and implementation of decoy state quantum key distribution over 60km telecom fiber.". International Symposium on Information Theory. IEEE, 2006.

[17] Data, Propagation. "Prediction Methods Required for the Design of Terrestrial Line-of-Sight Systems." Recommendation ITU-R (2007): 530.

[18] Giggenbach, D. , and Henniger H. "Fading-loss assessment in atmospheric free-space optical communication links with on-off keying." Optical Engineering 47.4 (2008): 046001.

[19] Uysal, M. , Li J. , and Yu M. "Error rate performance analysis of coded free-space optical links over gamma-gamma atmospheric turbulence channels." IEEE Transactions on wireless communications 5.6 (2006): 1229-1233.

[20] Korai, U. A., Luini L. ,et al. "Model for the prediction of rain attenuation affecting free space optical links." Electronics 7.12 (2018): 407.

[21] Recommendation ITU-R P. 1621, "Propagation data required for the design of Earth-space systems operating between 20THz and 375 THz", 2003

[22] Rollins, D. , et al. "Background light environment for free-space optical terrestrial communications links." Optical Wireless Communications V. Vol. 4873. International Society for Optics and Photonics, 2002.

[23] http://www.koruza.net/specs/, Accessed on: 30/3/2021

[24] Nauerth, S., et al. "Air-to-ground quantum communication." Nature Photonics 7.5 (2013): 382-386.

[25] Hughes, R. J., et al. "Practical free-space quantum key distribution over 10 km in daylight and at night." NJOF 4.1 (2002): 43.

[26] Mlejnek, M., Nikolay A. Kaliteevskiy, and Dan A. Nolan. "Reducing spontaneous Raman scattering noise in high quantum bit rate QKD systems over optical fiber." arXiv preprint arXiv:1712.05891 (2017).

[27] Kourogiorgas, C. I., et al. "Dynamic properties of rain attenuation in Athens, Greece: slant path rain attenuation synthesizer and dynamic diversity gain." Progress In Electromagnetics Research 41 (2015): 43-50.

[28] https://www.worldweatheronline.com/athens-weather-averages/attica/gr.aspx, Accessed on: 30/3/2021

[29] Carrasco-Casado, A. , Manuel J., Sánchez-Pena, and Vergaz R. "CTA telescopes as deep-space lasercom ground receivers." IEEE Photonics Journal 7.6 (2015): 1-14.

[30] Ntanos, A. , et al. "QKD in Support of Secured P2P and P2MP Key Exchange for Low-Latency 5G Connectivity." 5GWF. IEEE, 2020.

[31] Zavitsanos, D., et al. "On the QKD Integration in Converged Fiber/Wireless Topologies for Secured, Low-Latency 5G/B5G Fronthaul." Applied Sciences 10.15 (2020): 5193.